PAN
ARCHIVES OF ACOUSTICS
Vol. **46**, No. 2, pp. 341–352 (2021)
DOI: 10.24425/aoa.2021.136573

Research Paper

Experimental Assessment of the Impact of Sonication Parameters on Necrotic Lesions Induced in Tissues by HIFU Ablative Device for Preclinical Studies

Łukasz FURA[(1)], Wojciech DERA[(2)], Cezary DZIEKOŃSKI[(2)], Maciej ŚWIĄTKIEWICZ[(3)], Tamara KUJAWSKA[(1)*]

[(1)] *Department of Ultrasound*
Institute of Fundamental Technological Research
Polish Academy of Sciences
Warsaw, Poland
*Corresponding Author e-mail: tkujaw@ippt.pan.pl

[(2)] *Department of Theory of Continuous Media and Nanostructures*
Institute of Fundamental Technological Research
Polish Academy of Sciences
Warsaw, Poland

[(3)] *Department of Experimental Pharmacology*
Mossakowski Medical Research Centre
Polish Academy of Sciences
Warsaw, Poland

(*received September 23, 2020; accepted February 3, 2021*)

We have designed and built ultrasound imaging-guided HIFU ablative device for preclinical studies on small animals. Before this device is used to treat animals, *ex vivo* tissue studies were necessary to determine the location and extent of necrotic lesions created inside tissue samples by HIFU beams depending on their acoustic properties. This will allow to plan the beam movement trajectory and the distance and time intervals between exposures leading to necrosis covering the entire treated volume without damaging the surrounding tissues. This is crucial for therapy safety. The objective of this study was to assess the impact of sonication parameters on the size of necrotic lesions formed by HIFU beams generated by 64-mm bowl-shaped transducer used, operating at 1.08 MHz or 3.21 MHz. Multiple necrotic lesions were created in pork loin samples at 12.6-mm depth below tissue surface during 3-s exposure to HIFU beams with fixed duty-cycle and varied pulse-duration or fixed pulse-duration and varied duty-cycle, propagated in two-layer media: water-tissue. After exposures, the necrotic lesions were visualized using magnetic resonance imaging and optical imaging (photos) after sectioning the samples. Quantitative analysis of the obtained results allowed to select the optimal sonication and beam movement parameters to support planning of effective therapy.

Keywords: automated ultrasound imaging-guided HIFU ablation system; *ex vivo* tissue; ultrasonic exposure parameters; extent of necrotic lesions.

1. Introduction

Imaging-guided High-Intensity Focused Ultrasound (HIFU) ablative technique is a promising technology for thermal destruction of deeply localized solid tumors. This technique is dynamically developing due to its non-invasive (without surgical intervention) nature, lack of ionization, the possibility of repeated treatment and minimal side effects. The principle of this technique is very quick heating (<3 seconds) a small local volume inside the treated tissue (depending on the focal volume of the HIFU beam) to a temperature above 56°C, which leads to its coagulative necrosis (ter Haar, 2007). It is capable of ablating the tumor via

thermal and cavitational mechanisms, without damaging tissues surrounding the tumor (Ebbini, 2015). In recent years HIFU therapy has been successfully used clinically to treat prostate tumors (Guillaumier *et al.*, 2018; Veereman *et al.*, 2015), uterine fibroids (Zhang *et al.*, 2014; 2017; Shui *et al.*; 2015) or liver tumors (Leslie *et al.*, 2012, Zavaglia *et al.*, 2013).

To monitor the delivery of energy, concentrated in the focal volume of the HIFU beam, to the targeted volume inside the treated tissue both the magnetic resonance imaging (MRI) and ultrasound imaging (USI) is used. The advantage of MRI-guided HIFU (MRI-gHIFU) ablation systems over USI-guided ones (USI-gHIFU) is better imaging quality and the ability to monitor the temperature map in the targeted area in quasi-real time (Li *et al.*, 2013). However, the time of treatment procedure using MRI-gHIFU systems is much longer than that using USI-gHIFU devices (Wang *et al.*, 2018). In addition, USI-gHIFU systems allow to monitor treatment in real-time by feedback from hyper-echogenic area on ultrasound image (Yu *et al.*, 2008; Fukuda *et al.*, 2011). Also, the price and operating costs of MRI-gHIFU devices are much higher than those for the USI-gHIFU systems, which limits their wide application (Orsi *et al.*, 2010).

In most commercial ablative imaging-guided HIFU devices, multi-element phased arrays are used to generate HIFU beams with multiple foci controlled electronically in space and time (Choi *et al.*, 2014; Hand *et al.*, 2009; Melodelima *et al.*, 2009; Ellens *et al.*, 2015; Li *et al.*, 2018). However, they require multichannel electronics and complex software, which further increase the costs of such devices.

Therefore, many ultrasound laboratories would benefit from an inexpensive, USI-gHIFU ablative device with high stability and positioning accuracy to support the planning, monitoring and treatment of solid tumors in small animals during preclinical studies (Chauhan, 2008; Masamune *et al.*, 2013). This motivated us to develop, design and build a low-cost compact US-gHIFU ablation system to destroy solid tumors implanted in small animals and to test new anti-cancer drugs. Our device combines:

1) treatment planning and monitoring under the control of ultrasound imaging,
2) positioning the focus of the HIFU beam in the intended volume inside the treated tissue,
3) its computer-controlled movement, and
4) the performance of the procedure.

When planning ablation, information about the location and extent of the necrotic lesion induced by a single exposure to the HIFU beam is needed. This information is crucial for programming the beam movement trajectory and the distance and time intervals between exposures leading to the necrosis covering the entire treated volume inside the tissue.

In this study, the impact of the acoustic properties of the HIFU beam generated by our device on the location and extent of the necrotic lesion formed inside the examined tissue *ex vivo* was investigated. The quantitative analysis of the location and size of the necrotic lesions formed was made by visualizing them using the MR imaging as well as optical imaging (photos) after sectioning the tissue sample. In this study the ultrasound imaging was used only to pre-control the ablation procedure. It was used during HIFU ablation only to check whether a central necrotic lesion (visible as a hyperechoic area) is formed on the axis of the ultrasound image of the axial section of the tissue sample at an intended depth below its surface.

These studies were intended to help in selecting the optimal HIFU beam parameters and to plan the trajectory of the HIFU beam movement when scanning the treated tissue volume as well as the distance and time intervals between exposures, leading to necrosis covering the entire treated volume without damaging the surrounding tissue structures. Correctly selected acoustic properties of the HIFU beam, trajectory of its movement during scanning and intervals (distance and time) between exposures result in the merging of necrosis areas induced by a single exposure. This is crucial for the safety of the therapy.

2. Materials and methods

2.1. Experimental setup

Block diagram of the experimental setup used is shown in Fig. 1.

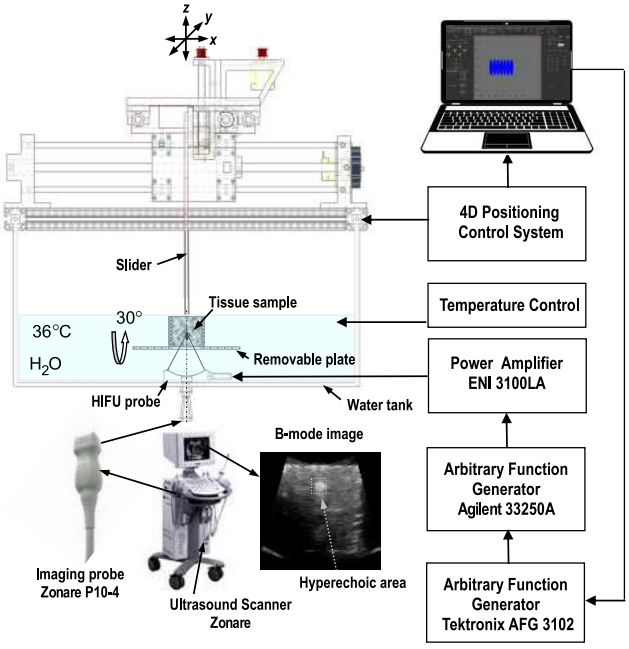

Fig. 1. Block diagram of the experimental setup for creating necrotic lesions inside tissue.

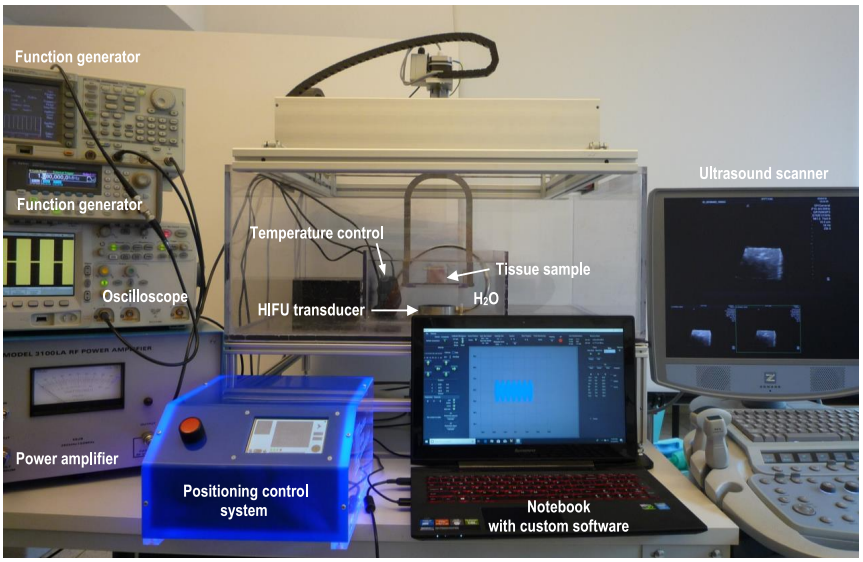

Fig. 2. Photo of the experimental setup for creating local necrotic lesions inside *ex vivo* tissues.

Our device combined the HIFU ablation system, ultrasound imaging system, automated positioning control system and computer with custom software. The HIFU ablation system included the HIFU probe driven by sinusoidal pulses generated by an Agilent 33250A function generator (Colorado Springs, USA) and amplified by the ENI 3100LA (55 dB) power amplifier (Rochester, New York, USA). In order for this generator to trigger the same number of pulses during each individual sonication and deliver the same energy to each local ablated tissue volume, the AFG 3102 function generator (Tektronix Inc., Beaverton, OR USA) was used. The waveforms were displayed using an MSO6052A mixed-signal oscilloscope (Agilent Technologies, Santa Clara, CA USA). The ultrasound imaging system contained a Zonare ultrasound scanner (Zonare Medical Systems Inc., Mountain View, CA, USA) equipped with a Zonare P10-4 phased array imaging probe. The probe bandwidth was 4–10 MHz. Ultrasonic imaging was performed at 4 MHz and at the second harmonic (8 MHz). The imaging probe had 128 elements and its radiating aperture dimensions were 11×18 mm. Figure 2 shows a photo of our robotic USI-guided HIFU ablation device for preclinical studies on small animals.

The HIFU probe, integrated coaxially with the ultrasound imaging probe, was mounted in a bottom of a water tank. A frame with a removable plate for positioning a treated animal or a tissue sample embedded in a reference cylindrical chamber was placed over the HIFU probe and connected to the slider of the precise positioning system enabling its mechanical movement in x, y, z directions and at a selected angle of inclination. The plate had a 50 mm circular hole (aligned coaxially with the heating and imaging probes integrated) through which the HIFU beam could penetrate the animal's body or tissue sample examined. The tissue chamber was immersed in the degassed water filling the water tank and serving both as a matching layer between the HIFU probe and the animal body or tissue sample, and as a cooling layer to prevent skin burns. The temperature of the water and tissue sample was controlled using an Aquael 100 electric heater (Aquael Sp. z o.o. Warsaw, Poland) and aquarium pump placed in the water tank. All measurements were carried out at a water and tissue temperature of 36°C. The HIFU beam energy, concentrated in the focal spot located inside the tissue, induced a local increase in temperature leading to the formation of a single necrotic lesion. The extent of the lesion produced depends on the size of the focal volume of the beam used. Multiple exposure of each tissue sample to HIFU beams with selected properties was carried out automatically after programming the trajectory of movement of the tissue chamber and the time and distance intervals between exposures.

2.2. HIFU probe

In our ablation device, a bowl-shaped H-102 transducer (Sonic Concepts Inc, Bothell, WA, USA) with an effective diameter of 64 mm, focal length of 62.6 mm (f-number 0.98) and operating frequency of 1.08 MHz or 3.21 MHz was used. The transducer had a 20 mm central opening for an imaging probe, custom 50 Ω matching circuits and was driven by sinusoidal pulses with a selected voltage, duration and duty-cycle. The admittance (module and phase) of this transducer, measured in water with the Agilent 4395A Impedance Analyzer (Agilent Technologies Inc, Colorado Springs, CO, USA), showed that its fundamental and 3rd harmonic resonance frequencies were 1.053 MHz and

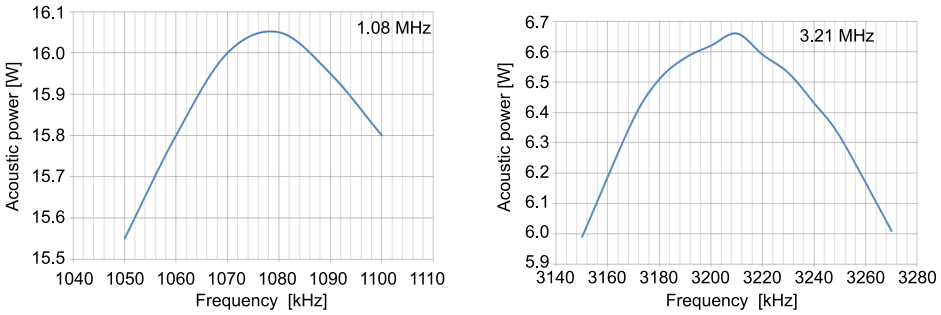

Fig. 3. The frequency dependence of the average acoustic power of the HIFU transducer to determine the resonance (1.08 MHz) and 3rd harmonic (3.21 MHz) operating frequencies.

3.34 MHz, respectively. According to the manufacturer's data-sheet these values were 1.1 MHz and 3.3 MHz, respectively. However, measurements of the average sound power of this transducer depending on the frequency using the UPM DT 1E ultrasonic power meter (Ohmic Instruments, St. Charles, MO, USA) showed that the maximum power HIFU beam was generated at a 1.08 MHz frequency (fundamental) and 3.21 MHz (3-rd harmonic) as shown in Fig. 3. Therefore these values were used in experiments.

2.3. HIFU beam characteristics in water

HIFU beam patterns in water were measured at room temperature (23°C) using a SN 1664 needle hydrophone (Precision Acoustics Ltd, Dorchester, Dorset, UK) with an active element diameter of 0.075 mm. For the safety of the hydrophone, the axial and radial pressure distributions in water were measured for a 1.08 MHz HIFU beam with an acoustic power of 16W evaluated for 0.2 duty-cycle. To generate such a beam, the excitation voltage applied to the transducer was 210 V_{pp}. The obtained data was compared with the results calculated with the nonlinear propagation model used in the k-Wave software available in the MatLab toolbox and described in (Treeby *et al.*, 2012). The best agreement between the simulated results and measured data allowed to determine the source pressure, the peak-positive and peak-negative pressure in the beam used as well as its focal intensity I_{SATA} and the size of the focal volume of the beam. The calculated and measured axial and radial pressure distributions in the HIFU beam with 16 W acoustic power generated in water are shown in Fig. 4.

For this HIFU beam, the initial (source), peak-positive, and peak-negative pressures calculated in water were found to be 0.273 MPa, 10.5 MPa, and 6.3 MPa, respectively. The focal intensity I_{SATA} calculated from the radial peak-positive pressure distribution for −6 dB beam width was about 0.8 kW/cm^2. The −6 dB length and diameter of the ellipsoidal focal volume of the HIFU beam were about 11 mm and 1.4 mm, respectively.

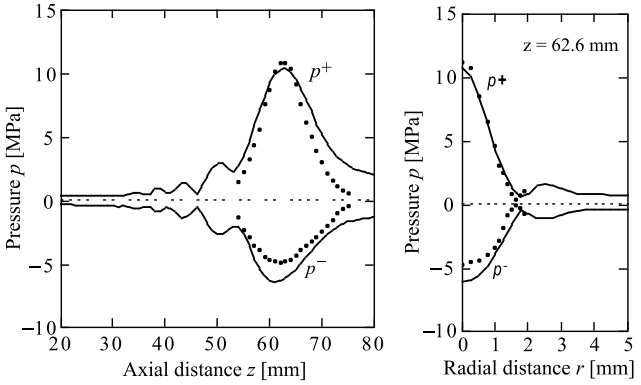

Fig. 4. Calculated (solid lines) and measured (points) axial (left) and radial (right) peak-positive p^+ and peak-negative p^- pressure distributions in 16 W HIFU beam with 1.08 MHz frequency generated in water.

2.4. Preparation of tissue samples

The tissue samples were prepared from a fresh pork loin purchased from a local butcher. The samples were cut with a cylindrical knife into blocks, then degassed and embedded into a cylindrical chamber with an outer diameter of 50 mm, internal diameter of 45 mm and height of 40 mm. To prevent the water-tissue surface from folding, the chamber had sound-transparent windows made of 20-μm thick Mylar film stretched tightly at each its end.

2.5. Media of propagation

As shown by the design of our device, HIFU beams were generated in two-layer media of propagation consisting of water and tissue examined. In order to maximize the effect of harmonics on the focal intensity of the beam and on the temperature rise induced locally inside the tissue, the thickness of the water layer was selected from the above-mentioned model of non-linear propagation in water. The thickness of the water layer was determined as the axial distance from the transducer, at which the second harmonic amplitude begins to rise rapidly (Wójcik *et al.*, 2006; Kujawska *et al.*, 2017). For the transducer used here this distance was

found to be 50 mm. Accordingly, each beam was propagated in two-layer media containing water (50 mm) and pork loin (40 mm) and focused inside the tissue at a depth of 12.6 mm below its surface.

2.6. HIFU beam sound power selection

The threshold sound power of the HIFU beam capable of creating a local necrotic lesion inside the examined tissue in less than 3 s, was determined in our previous publication (Fura *et al.*, 2019) and was 24 W (measured for 0.2 duty-cycle). In those studies a HIFU transducer with the same frequency and geometry but without a central hole was used. Other experimental conditions were the same. Therefore, to produce HIFU beams of the same average acoustic power with the transducer used here (with a central hole) the higher excitation voltage was needed. As we intend to use this transducer to treat tissues *in vivo* where the delivery of acoustic energy is more difficult due to blood perfusion, HIFU beams with higher sound power (36 W for 1.08 MHz beams and 17.1 W for 3.21 MHz beams) measured for a 0.2 duty-cycle were used in this study. To generate such beams, the excitation voltage applied to the transducer was 371 V_{pp}.

2.7. HIFU beam characteristics in tissue

In order to determine the intensity of the applied HIFU beam in its focal plane located inside the examined tissue, its propagation in two-layer media: water–tissue (50 mm – 40 mm) was numerically simulated using mentioned above k-Wave non-linear propagation model and assuming the acoustic properties of propagation media known from the literature. The assumed acoustic parameters of pork loin, being the input data required for the model, were: 1060 kg/m^3 density (Duck, 1990), 1615 m/s sound velocity (Koch *et al.*, 2011), $11 \cdot 10^{-6}$ Np/(m$\cdot$Hz^b) attenuation coefficient (Koch *et al.*, 2011), where power index of frequency-dependent attenuation b = 1.1 (Nassiri *et al.*, 1979) and nonlinearity parameter B/A = 8 (Law *et al.*, 1985). The focal intensity I_{SATA} of the HIFU beam inside the tissue was also determined from the radial peak-positive pressure distribution for −6 dB beam width.

For 1.08 MHz HIFU beams with 36 W sound power (measured for 0.2 duty-cycle) the calculated focal intensity I_{SATA} inside the tissue was found to be 3.2 kW/cm^2. For 3.21 MHz HIFU beams with the 17.1 W sound power (for the same excitation voltage), this intensity was 5.9 kW/cm^2. Quantitative analysis of the results obtained from the numerical simulations allowed to determine the length and diameter of the ellipsoidal focal volume of the HIFU beams used. The obtained results showed that for the 1.08 MHz beams the length of their focal volume inside the tissue was about 9 mm and the diameter 1.2 mm, while for the 3.21 MHz beams, these values were approximately 3.4 mm and 0.5 mm, respectively.

2.8. HIFU device alignment

To create multiple necrotic lesions inside each tissue sample, the tissue chamber was placed in a circular hole of the plate inserted into the frame and immersed in water. Prior to sonication, our ablation system was aligned to ensure both the coaxiality of the HIFU probe with the tissue chamber and the axial distance between them. The measurements were performed using 0.075 mm needle hydrophone placed at the center of the circular hole of the plate immersed in water.

2.9. HIFU beam positioning configuration

The 1.08 MHz or 3.21 MHz HIFU beams propagated in two-layer media water–tissue (50 mm – 40 mm) were investigated. The beams of the same frequency were divided into 2 groups, 3 different beams per group. Each group of 3 beams of the same frequency was used to sonicate one tissue sample. The first group consisted of 3 beams with fixed duty-cycle (0.6) and varied pulse duration (30 µs; 3 ms; 0.3 s). The second group consisted of 3 beams with fixed pulse duration (0.3 s) and varied duty-cycle (0.4; 0.6; 0.8). The duration of each sonication was 3 s. The exposure time and the number of pulses delivered to each targeted volume inside the tissue were controlled using our custom software.

To maximize the use of each tissue sample and the amount of statistical data collected, each sample was sonicated on both sides, with 5 exposures on each side for each of the 3 beams per group. Therefore, after each sample was sonicated with 3 beams from the same group, 30 necrotic lesions were formed, 10 for each beam from the selected group. In the experiment with each group of beams of the same frequency, 2 samples were involved, for a total of 8 samples. Hence, a total of 240 necrotic lesions were analyzed.

As mentioned above, for each HIFU beam with selected acoustic parameters, 10 parallel necrotic lesions were created inside the tissue sample in the xz plane, 5 on each side. Each sample was sonicated by 3 different HIFU beams from the selected group in 3 parallel xz planes spaced 5 mm apart in the y direction as shown in Fig. 5.

As is clear from the geometry of the two-layer system of propagation media, the HIFU beams were focused inside each tissue sample at a depth of 12.6 mm below its surface. Multiple necrotic lesions were created inside the tissue by moving the tissue chamber 5 times along the x axis at 2.5-mm intervals between exposures.

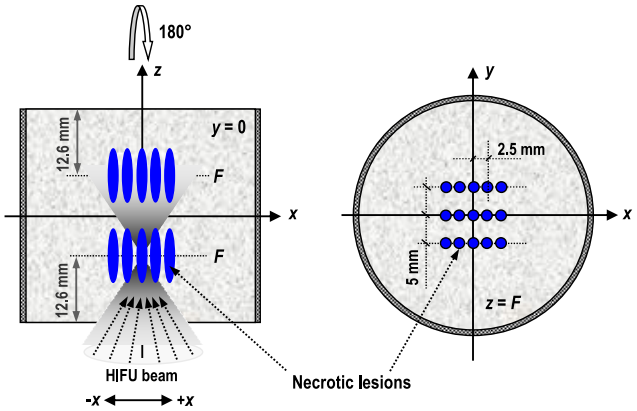

Fig. 5. Diagram of the axial (left) and radial (right) – in the focal plane of the HIFU beam – distribution of necrotic lesions planned to be created inside each tissue sample.

2.10. Visualization of necrotic lesions

After sonication, the necrotic lesions created inside each tissue sample were visualized in the axial and focal planes by B-mode ultrasound imaging using Zonare ultrasound scanner (Zonare Medical Systems Inc., Mountain View, CA, USA) equipped with P10-4 and L14-5w imaging probes as well as by T1-weighted magnetic resonance imaging using Bruker Biospec 70/30USR magnetic resonance scanner with 7T induction of magnetic field (Bruker Polska Sp. z o.o., Poznań, Poland).

The location and extent of thermal lesions, visible as hyper-echogenic areas on ultrasound images and dark areas on T1-weighted magnetic resonance images, were identified and compared with those visible after dissection of the tissue sample. The MR images obtained were pre-processed with OsiriX Lite software (Pixmeo SARL, Switzerland) to create a single image with minimum-intensity projection (MinIP) area (corresponding to necrosis) from the sequence of MR images covering the entire volume of the necrotic lesion.

Then, each tissue sample embedded in the cylindrical chamber was frozen for about 2 hours at −18°C to make it easier to cut. Next, each hardened tissue sample was removed from the chamber and sectioned to make the lesions visible at their maximum length and diameter. The extent and location of lesions were assessed from their axial and radial cross-sectional photos using the Java-based image processing program ImageJ (Schneider *et al.*, 2012). The length and diameter of each lesion were presented as a function of the exposure parameters (frequency, pulse duration, duty-cycle) of the HIFU beams used.

2.11. Statistical analysis of results

The location and extent of thermal lesions, visible as hyper-echogenic areas on ultrasound images and dark areas on T1-weighted magnetic resonance images, were identified and compared with those visible after dissection of each tissue sample. The mean value of the position of the center of the necrotic lesions and their size was determined along with the standard deviations. Linear functions were fitted to the measured values of the length and diameter of necrotic lesions using the least squares method. Pearson's linear correlation coefficient was calculated to assess the relationship between the acoustic properties of the HIFU beam and the lesion location and extent. The greater the correlation between the variables, the higher was the absolute value of this coefficient.

Data were analyzed using R programming language. As mentioned above, the number of necrotic lesions analyzed for all applied HIFU beams with selected parameters was 240. Results were expressed as mean values ±standard deviation (σ).

3. Results and discussion

Based on a quantitative analysis of the obtained experimental results, the location and extent of the ellipsoidal necrotic lesions, created in the tested tissue by the HIFU beams used, were evaluated depending on the beam frequency, pulse duration and duty-cycle as well as on the distance and time intervals between exposures. The analysis was performed by visualizing the axial and radial sections of the lesions formed using various imaging methods (ultrasound, magnetic resonance and optical imaging) and by comparing the results.

Figure 6 shows an exemplary ultrasound image of the axial section of the central necrotic lesion created in the examined tissue during its exposure to the 3.21 MHz HIFU beam. The ultrasound imaging probe frequency of 8 MHz and the imaging depth of 10 cm was used.

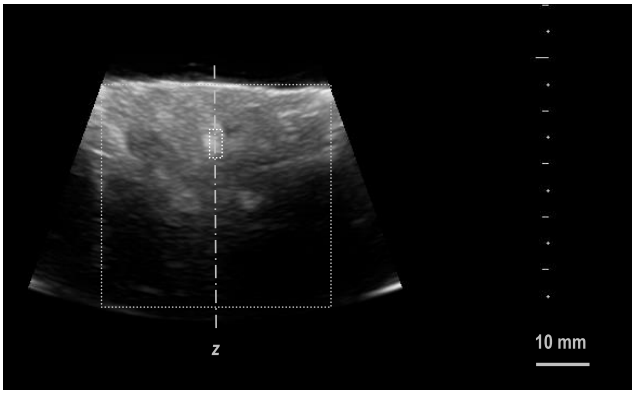

Fig. 6. Ultrasound image of the axial section (xz) of the central necrotic lesion created by the HIFU beam (with a 3.21 MHz frequency, 0.3 s pulse duration and 0.6 duty-cycle) in the tissue sample at a 12.6 mm depth below the tissue surface. The tissue chamber outline is marked with a larger rectangle, the hyper-echogenic area is marked with a small rectangle.

As can be seen from Fig. 6, the hyperechoic area appeared on the axis of the ultrasound image at the intended depth under the tissue surface, which proves the coaxiality of the formed central necrotic lesion with the ultrasound image of the axial section of the tissue chamber.

3.1. Impact of HIFU beam frequency

The influence of the HIFU beam frequency on the extent of created necrotic lesions was examined. For this purpose, 1.08 MHz or 3.21 MHz HIFU beams with the same duty-cycle (DC = 0.6) and varied pulse duration ($\Delta\tau$ = 30 μs; 3 ms; 0.3 s) as well as with the same pulse duration ($\Delta\tau$ = 0.3 s) and varied duty-cycle (DC = 0.4; 0.6; 0.8) were studied. In Figs 7 and 8 the axial cross-sectional area of the necrotic lesions formed and visualized respectively by the optical (photos) and magnetic resonance (images) imaging methods are shown.

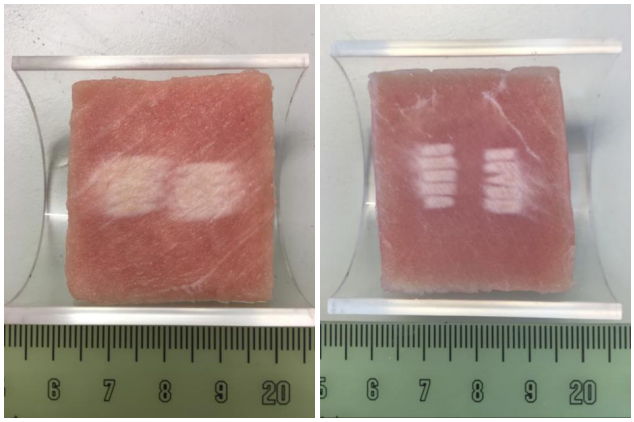

Fig. 7. Photos of axial sections of 10 necrotic lesions created in the tissue sample after its sonication on both sides by 5 HIFU beams with 1.08 MHz (left) or 3.21 MHz (right) frequency, 0.3 s pulse duration and 0.6 duty-cycle.

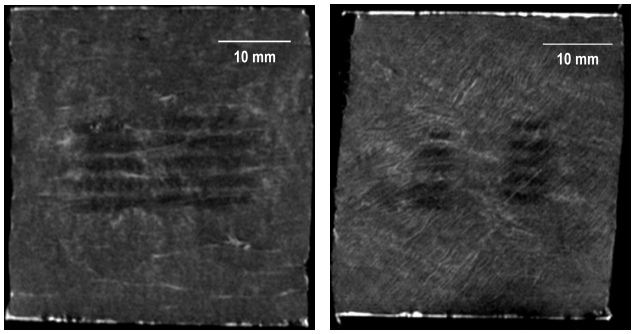

Fig. 8. T1-weighted MR images of axial sections of 10 necrotic lesions created in the tissue sample after its sonication on both sides by 5 HIFU beams with 1.08 MHz (left) or 3.21 MHz (right) frequency, 0.3-s pulse duration and 0.6 duty-cycle.

Quantitative analysis of the results of measuring the length and diameter of the created necrotic lesions, obtained from photos and MR images of their cross-sections, showed that the lesion length strongly depends on frequency of the HIFU beam used and is close to the one calculated (within ±9%). As it can be seen from our calculations presented above, for HIFU beams with a frequency of 3.21 MHz the length and diameter of their ellipsoidal focal volume is more than twice smaller than for the 1.08 MHz beams. However, the results of measurements of the size of the necrotic lesions formed showed that, while the length of the lesions was actually about 2 times smaller, their diameter was much larger than that resulting from the calculations. This is most likely due to the fact that although the 3.21 MHz beams have lower acoustic power and source pressure, their focal intensity is more than three times higher than that of the 1.08 MHz beams. In the case of linear propagation, the focal gain for these beams is 110 and 36, respectively. Considering the fact that the calculated −6 dB width of the 3.21 MHz beams in the focal plane is much smaller, its energy is concentrated on a smaller focal area. This leads to a much higher focal intensity compared to the 1.08 MHz beams. Conversely, higher focal intensity leads to a faster and greater increase in temperature inside the tissue. Due to the higher temperature gradient, the heat diffusion is also faster, leading to more extensive thermal damage to the tissue at the same exposure time.

Table 1 presents the average values of the length and diameter of the created lesion depending on the frequency of the HIFU beam used.

Table 1. The average values of the length and diameter of the necrotic lesion created inside the tissue by HIFU beams with the same pulse duration (0.3 s) and duty-cycle (0.6) and varied frequency, with standard ndeviation (σ).

			Mean value ±σ [mm]	
			Photo	MRI
$\Delta\tau$ = 0.3 s DC = 0.6	f = 1.08 MHz	length	10.9 ± 1.1	9.58 ± 0.80
		diameter	2.04 ± 0.18	1.69 ± 0.20
	f = 3.21 MHz	length	5.69 ± 0.52	4.70 ± 1.10
		diameter	1.94 ± 0.15	1.35 ± 0.36

Comparing the values of the lesion length and diameter obtained from photos with those obtained from MR images, it was found that they are compatible with each other within the standard deviation. Figure 9 presents the dependence of the lesion length and diameter on the frequency of the HIFU beam used, determined from photos and MR images, along with the function described by a linear equation, fitted using the least squares method.

The calculated coefficients for the linear function described by the equation $y(f) = a \cdot f + b$ along with the Pearson linear correlation coefficient (r) are shown in Table 2.

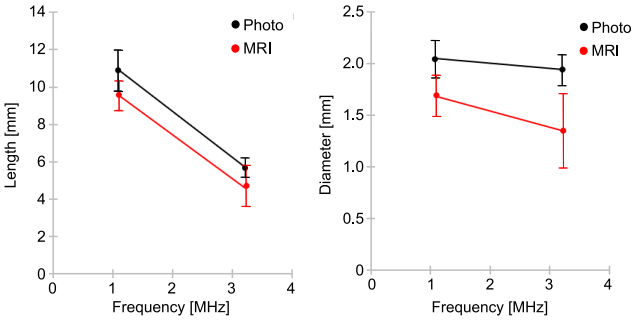

Fig. 9. The length (left) and diameter (right) of lesions measured from photos (black dots) and MR images (red dots) and modeled using linear equations (solid lines of appropriate color) depending on the frequency of the HIFU beam used.

Table 2. Pearson's correlation coefficients (r) and linear equation coefficients a and b with their standard deviations σ (a) and σ (b), determined from photos and MR images.

f [MHz]		r	a	σ (a)	b	σ (b)	Equation
Photo	length	−0.96	−2.46	0.17	13.59	0.45	$y = a \cdot f + b$
	width	−0.31	−0.050	0.021	2.10	0.055	
MRI	length	−0.94	−2.34	0.13	12.11	0.32	
	width	−0.46	−0.160	0.037	1.86	0.10	

Based on the quantitative analysis of the obtained results, a correlation between the length of the lesion created and the HIFU beam frequency was demonstrated.

3.2. Impact of pulse duration

The effect of pulse duration of the HIFU beam used on the extent of the lesion formed was also investigated. Photos and MR images of an exemplary axial and radial (in the focal plane) cross-sections of the necrotic lesions created inside the examined tissue after sonication by HIFU beams of the same frequency and duty-cycle and varied pulse duration are shown respectively in Figs 10 and 11.

From measurements of the length and diameter of created lesions, estimated from photos and MR images, their average values were determined. Quantitative analysis of the obtained results showed that for the HIFU beams used, with the same frequency and duty-cycle but varied pulse duration increasing in 100 and 10 000 times, the lesion size was very similar. This can be explained by the fact that the beams of the same frequency, acoustic power and duty-cycle have the same focal intensity I_{SATA} responsible for the increase in temperature and heat diffusion rate. Figure 12 presents the average values of the lesion length and diameter measured from photos and MR images and modeled by linear function. The calculated coefficients of the linear equation $y(\Delta\tau) = a \cdot \log(\Delta\tau) + b$ along with the Pearson linear correlation coefficients (r) are shown in Table 3.

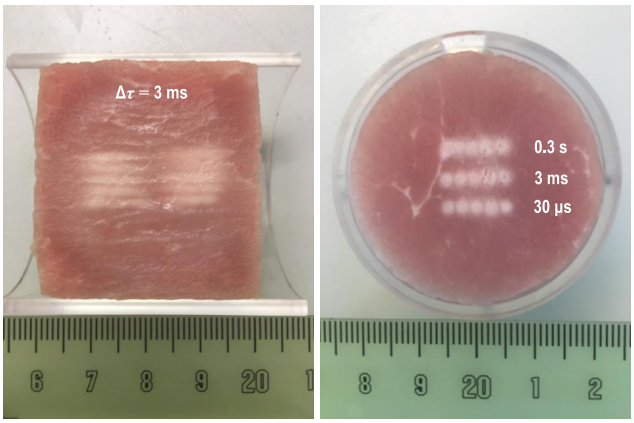

Fig. 10. Photos of the axial (left) and radial (right) – in the focal plane – cross-sections of the necrotic lesions formed inside the tissue after repeated 3 s exposure on both sides to 5 HIFU beams with a 1.08 MHz frequency, 0.6 duty-cycle and varied pulse duration: 30 µs (bottom); 3 ms (center); 0.3 s (top).

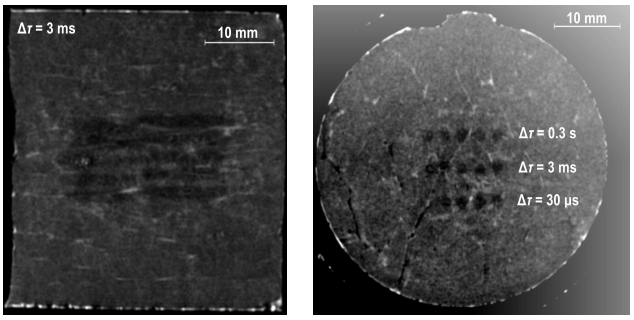

Fig. 11. T1-weighted MR images of the axial (left) and radial (right) – in the focal plane – cross-sections of the necrotic lesions formed inside the tissue after its repeated 3 s exposure on both sides to 5 HIFU beams with a 1.08 MHz frequency, 0.6 duty-cycle and varied pulse duration: 30 µs (bottom); 3 ms (center); 0.3 s (top).

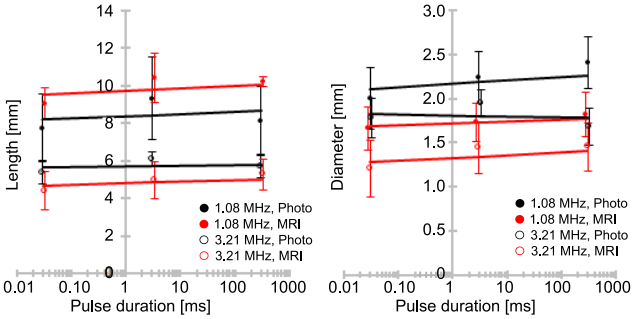

Fig. 12. The length (left) and diameter (right) of the lesion created by the HIFU beams with 1.08 MHz (dots) or 3.21 MHz (circles) frequency, 0.6 duty-cycle and varied pulse duration (30 µs; 3 ms; 0.3 s) and measured from photos (black symbols) or MR images (red symbols) as well as modeled by linear function fitted to the measured data.

Table 3. Pearson's linear correlation coefficients (r) and coefficients of the linear model (a, b) along with their standard deviations $\sigma(a)$, $\sigma(b)$ determined from the photos and MR images to describe the relationship between the lesion length and diameter and the pulse duration ($\Delta\tau$) in the HIFU beam.

			r	a	$\sigma(a)$	b	$\sigma(b)$	Equation
f = 1.08 MHz DC = 0.6	Photo	length	0.31	0.115	0.075	8.37	0.25	$y = a \cdot \log(\Delta\tau) + b$
		width	0.46	0.0441	0.0093	2.169	0.035	
	MRI	length	0.26	0.13	0.058	9.72	0.23	
		width	0.28	0.018	0.005	1.718	0.022	
f = 3.21 MHz DC = 0.6	Photo	length	0.20	0.032	0.024	5.689	0.094	
		width	−0.213	−0.013	0.0084	1.814	0.031	
	MRI	length	0.35	0.091	0.027	4.80	0.11	
		width	0.32	0.026	0.006	1.331	0.026	

3.3. Impact of duty-cycle

Then, the influence of the duty cycle (DC) of the HIFU beam on the length and diameter of the lesions formed was examined. Experiments were carried out for 1.08 MHz or 3.21 MHz beams with the same 0.3 s pulse duration but varied duty-cycle (DC = 0.4; 0.6; 0.8). The results of measurements of the axial and radial (in the focal plane) sections of necrotic lesions from photos and MR images allowed to determine the average size of these lesions. Sample photos and MR images of axial and radial sections of necrotic lesions formed in the examined tissue by 3 different HIFU beams of the same frequency and pulse duration, but with varied duty-cycle, are shown in Figs 13 and 14, respectively.

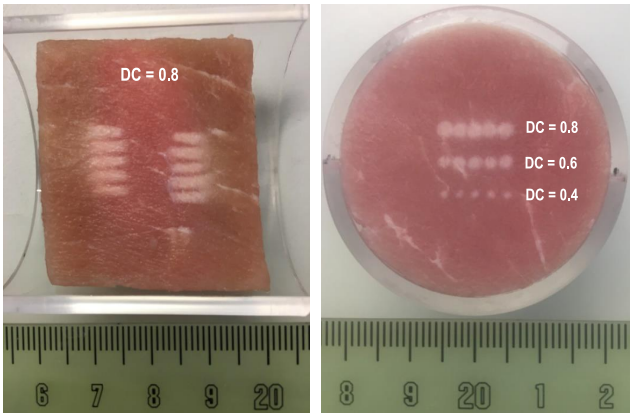

Fig. 13. Photos of axial (left) and radial (right) – in the focal plane - sections of lesions formed inside the tissue sample by 5 HIFU beams of 3.21 MHz frequency, 0.3 s pulse duration and varied duty-cycle: 0.4 (bottom); 0.6 (middle) and 0.8 (top).

After determining the length and diameter of the created lesions, measured from photos and MR images, their average size was calculated. Quantitative analysis of the obtained results showed that both the lesion length and diameter increased with increasing the duty-cycle of the HIFU beam. This is most likely due to a longer effective exposure time leading to longer diffusion of heat due to shorter intervals between pulses reducing the tissue cooling time. Figure 15 presents the measured from photos and MR images and modeled length and diameter of lesions created by HIFU beams with the same frequency and pulse duration, but with a varied duty-cycle. The linear function was fitted to the measurement results using the least squares method.

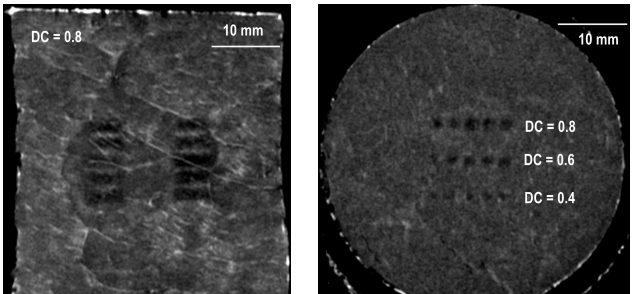

Fig. 14. T1-weighted MR images of axial (left) and radial (right) – in the focal plane – sections of lesions formed inside the tissue sample by 5 HIFU beams with a frequency of 3.21 MHz, pulse duration of 0.3 s, and duty-cycle varied: 0.4 (bottom); 0.6 (middle) and 0.8 (top).

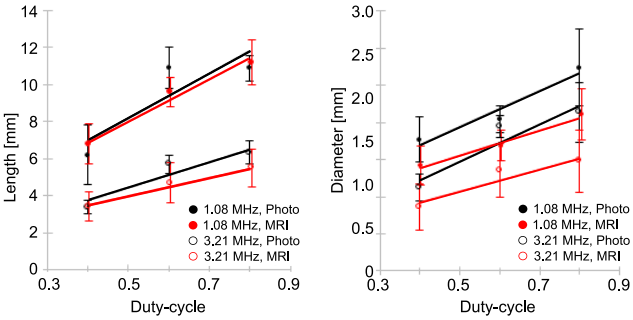

Fig. 15. Length (left) and diameter (right) of the created lesions, measured from photos (black symbols) or MR images (red symbols) and modeled by linear functions fitted to the measured data (solid lines of appropriate color). The lesions were formed by 1.08 MHz (dots) or 3.21 MHz (circles) HIFU beams with 0.3-s pulse duration and varied duty-cycle (0.4; 0.6; 0.8).

Table 4. Pearson's linear correlation coefficients (r) and linear function coefficients (a, b) along with their standard deviations $\sigma(a)$, $\sigma(b)$ determined to describe the dependence of the lesion length and diameter on duty-cycle of the HIFU beam.

			r	a	$\sigma(a)$	b	$\sigma(b)$	Equation
f = 1.08 MHz $\Delta\tau$ = 0.3 s	Photo	length	0.77	12.2	2.3	2.1	1.4	$y = a \cdot \mathrm{DC} + b$
		width	0.74	2.39	0.29	0.75	0.17	
	MRI	length	0.87	11.19	0.91	2.45	0.58	
		width	0.71	1.68	0.20	0.72	0.13	
f = 3.21 MHz $\Delta\tau$ = 0.3 s	Photo	length	0.86	6.90	0.61	0.99	0.41	
		width	0.80	2.49	0.19	0.23	0.12	
	MRI	length	0.69	5.05	0.60	1.45	0.39	
		width	0.53	1.48	0.19	0.34	0.13	

3.4. Impact of the distance and time intervals between exposures

Further factors that influenced the length and diameter of the lesions were the distance and time intervals between subsequent sonications. The results of our experiments showed that for HIFU beams with the same acoustic parameters, the length of the necrotic lesion formed depends on the distance between successive sonications. The distance between successive necrotic lesions was chosen to be 2.5 mm. Figure 16 shows photos of axial sections of necrotic lesions formed on both sides of the tissue sample by the applied HIFU beam, shifted along the x axis 5 times in series or steps, with the selected distance and time intervals.

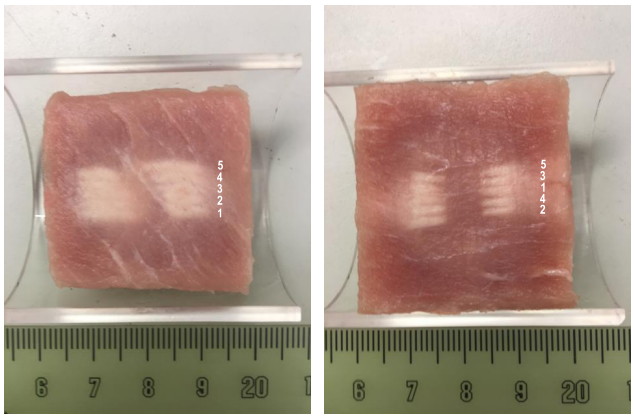

Fig. 16. Photos of axial sections of necrotic lesions formed by a 1.08-MHz HIFU beam with a 0.3-s pulse duration and 0.6 duty-cycle (left) and by a 3.21-MHz HIFU beam with the same pulse duration and duty-cycle (right), shifted 5 times in series every 2.5 mm in 40-s time intervals (left) or by leaps and bounds in 60-s time intervals (right).

The visualization of the axial sections of the created lesions showed that in the case of the serial sonications (Fig. 16 left) the lesion length increased while maintaining the same diameter. In the case of the step exposures (Fig. 16 right) the length and diameter of necrotic lesions remained practically the same. This phenomenon can be explained by the fact that for serial sonications, the initial tissue temperature at the site of the next ablation may be higher than that at the site of the previous ablation due to heat diffusion or insufficient time interval between sonications due to the relaxation time of the tissue. Therefore, when planning the shape and size of the targeted local volume inside the tissue subjected to ablation, this effect should be taken into account to avoid damage the surrounding untreated tissues.

As it results from the data obtained from the MR images, the size of the necrotic lesions formed is smaller than that measured from the photos. The reason for this is most likely because MRI is based on the phenomenon of nuclear magnetic resonance. The resonance nuclei used to reconstruct the MR image are protons found in water molecules contained in biological tissues. In T1-weighted MR images, areas with little water appear dark, while areas with a lot of water appear bright. The size of necrotic lesions measured from optical images was usually larger than that measured from MR images most likely because tissue discoloration in the photos does not necessarily indicate the same degree of dehydration and change in structure.

The quantitative analysis of the obtained measurement results made it possible to select the movement trajectory of the HIFU beams used and the distance and time intervals between exposures, which will be able to necrotize the entire targeted volume inside the examined *ex vivo* tissue without damaging the surrounding structures. For example, for 1.08 MHz beams with 0.6 duty-cycle the minimal distance between exposures was about 2 mm, while for 3.21 MHz beams with the same duty-cycle it was about 1.9 mm. The time intervals between sonications for these beams were 60 s.

4. Conclusions

Based on the results of the conducted experimental research, it was shown that our HIFU ablation device

guided by ultrasound imaging is able to create clearly outlined necrotic lesions in the targeted local volume inside the *ex vivo* tissue without damaging adjacent tissue structures. Quantitative analysis of the obtained data allowed to estimate the location and extent of the created necrotic lesions depending on the acoustic properties of the HIFU beams used (frequency, pulse duration, duty-cycle), as well as on the distance and time intervals between successive ablations. Based on this analysis, the beam movement trajectory as well as the distance and time intervals between exposures, could be determined for each HIFU beam capable of forming well-defined necrotic lesions in the targeted volume inside the examined tissue within 3-s exposure. This is crucial for assessing the targeting accuracy of this device and for future preclinical studies on animals.

Acknowledgements

This work was supported by the National Science Centre of Poland under Grant number 2016/21/B/ST8/02445.

References

1. Chauhan S. (2008), *FUSBOTs: image-guided robotic systems for Focused Ultrasound Surgery, Medical Robotics*, Vanja Bozovic, I-Tech Education and Publishing, Vienna, Austria.
2. Choi J.W. *et al.* (2014), Portable high-intensity focused ultrasound system with 3D electronic steering, real-time cavitation monitoring, and 3D image reconstruction algorithms: a preclinical study in pigs, *Ultrasonography*, **33**(3): 191–199, doi: 10.14366/usg.14008.
3. Duck F.A. (1990), *Physical Properties of Tissue: A Comprehensive Reference Book*, Academic Press, London.
4. Ebbini E.S., ter Haar G. (2015), Ultrasound-guided therapeutic focused ultrasound: current status and future directions, *International Journal of Hyperthermia*, **31**(2): 77–89, doi: 10.3109/02656736.2014.995238.
5. Ellens N. *et al.* (2015), The targeting accuracy of a preclinical MRI-guided focused ultrasound system, *Medical Physics*, **42**(1): 430–439, doi: 10.1118/1.4903950.
6. Fukuda H. *et al.* (2011), Hyper-echo in ultrasound images during high-intensity focused ultrasound ablation for hepatocellular carcinomas, *European Journal of Radiology*, **80**(3): e571–e575, doi: 10.1016/j.ejrad.2011.09.001.
7. Fura Ł., Kujawska T. (2019), Selection of exposure parameters for a HIFU ablation system using an array of thermocouples and numerical simulations, *Archives of Acoustics*, **44**(2): 349–355, doi: 10.24425/aoa.2019.128498.
8. Guillaumier S. *et al.* (2018), A multicentre study of 5-year outcomes following focal therapy in treating clinically significant nonmetastatic prostate cancer, *European Urology*, **74**(4): 422–429, doi: 10.1016/j.eururo.2018.06.006.
9. ter Haar G. (2007), Therapeutic applications of ultrasound, *Progress in Biophysics & Molecular Biology*, **93**(1–3): 111–129, doi: 10.1016/j.pbiomolbio.2006.07.005.
10. Hand J.W., Shaw A., Sadhoo N., Rajaqopal S., Dickinson R.J., Gavrilov L.R. (2009), A random phased array device for delivery of high intensity focused ultrasound, *Physics in Medicine & Biology*, **54**(19): 5675–5693, doi: 10.1088/0031-9155/54/19/002.
11. Koch T., Lakshmanan S., Brand S., Wicke M., Raum K., Moerlein D. (2011), Ultrasound velocity and attenuation of porcine soft tissues with respect to structure and composition: I. Muscle, *Meat Science*, **88**(1): 51–58, doi: 10.1016/j.meatsci.2010.12.002.
12. Kujawska T., Secomski W., Byra M., Postema M., Nowicki A. (2017), Annular phased array transducer for preclinical testing of anti-cancer drug efficacy on small animals, *Ultrasonics*, **76**: 92–98, doi: 10.1016/j.ultras.2016.12.008.
13. Law W.K., Frizzell L.A., Dunn F. (1985), Determination of the nonlinearity parameter B/A of biological media, *Ultrasound in Medicine & Biology*, **11**(2): 307–318, doi: 10.1016/0301-5629(85)90130-9.
14. Leslie T. *et al.* (2012), High-intensity focused ultrasound treatment of liver tumours: post-treatment MRI correlates well with intra-operative estimates of treatment volume, *The British Journal of Radiology*, **85**(1018): 1363–1370, doi: 10.1259/bjr/56737365.
15. Li K., Bai J.F., Chen Y.Z., Ji X. (2018), Experimental evaluation of targeting accuracy of an ultrasound-guided phased-array high-intensity focused ultrasound system, *Applied Acoustics*, **141**: 19–25, doi: 10.1016/j.apacoust.2018.06.011.
16. Li S., Wu P.H. (2013), Magnetic resonance image-guided versus ultrasound guided high-intensity focused ultrasound in the treatment of breast cancer, *Chinese Journal of Cancer*, **32**(8): 441–452, doi: 10.5732/cjc.012.10104.
17. Masamune K., Kurima I., Kuwana K., Yamashita H., Chiba T., Dohi T. (2013), HIFU positioning robot for less-invasive fetal treatment, *Procedia CIRP*, **5**: 286-289, doi: 10.1016/j.procir.2013.01.056.
18. Melodelima D., N'Djin W.A., Parmentier H., Chesnais S., Rivoire M., Chapelon J.Y. (2009), Thermal ablation by high-intensity-focused ultrasound using a toroid transducer increases the coagulated volume. Results of animal experiments, *Ultrasound in Medicine & Biology*, **35**(3): 425–435, doi: 10.1016/j.ultrasmedbio.2008.09.020
19. Nassiri D.K., Nicholas D., Hill C.R. (1979), Attenuation of ultrasound in skeletal muscle, *Ultrasonics*, **17**(5): 230–232, doi: 10.1016/0041-624x(79)90054-4.

20. Orsi F., Arnone P., Chen W., Zhang L. (2010), High intensity focused ultrasound ablation: a new therapeutic option for solid tumors, *Journal of Cancer Research and Therapeutics*, **6**(4): 414–420, doi: 10.4103/0973-1482.77064.

21. Schneider C.A., Rasband W.S., Eliceiri K.W. (2012), NIH Image to ImageJ: 25 years of image analysis, *Nature Methods*, **9**(7): 671–675, doi: 10.1038/nmeth.2089.

22. Shui L. *et al.* (2015), High-intensity focused ultrasound (HIFU) for adenomyosis: two-year follow-up results, *Ultrasonics Sonochemistry*, **27**: 677–681, doi: 10.1016/j.ultsonch.2015.05.024.

23. Treeby B.E., Jaros J., Rendell A.P., Cox B.T. (2012), Modeling nonlinear ultrasound propagation in heterogeneous media with power law absorption using a k-space pseudo-spectral method, *The Journal of the Acoustical Society of America*, **131**(6): 4324–4336, doi: 10.1121/1.4712021.

24. Veereman G. *et al.* (2015), Systematic review of the efficacy and safety of high-intensity focused ultrasound for localized prostate cancer, *European Urology Focus*, **1**(2): 158–170, doi: 10.1016/j.euf.2015.04.006.

25. Wang Y., Wang Z.B., Xu Y.H. (2018), Efficacy, efficiency, and safety of magnetic resonance-guided high-intensity focused ultrasound for ablation of uterine fibroids: comparison with ultrasound-guided method, *Korean Journal of Radiology*, **19**(4): 724–732, doi: 10.3348/kjr.2018.19.4.724.

26. Wójcik J., Nowicki A., Lewin P.A., Bloomfield P.E., Kujawska T., Filipczynski L. (2006), Wave envelopes method for description of nonlinear acoustic wave propagation, *Ultrasonics*, **44**: 310–329, doi: 10.1016/j.ultras.2006.04.001.

27. Yu T., Xu C. (2008), Hyperecho as the indicator of tissue necrosis during microbubble-assisted high intensity focused ultrasound sensitivity, specificity and predictive value, *Ultrasound in Medicine & Biology*, **34**(8): 1343–1347, doi: 10.1016/j.ultrasmedbio.2008.01.012.

28. Zavaglia C., Mancuso A., Foschi A., Rampoldi A. (2013), High-intensity focused ultrasound (HIFU) for the treatment of hepatocellular carcinoma: is it time to abandon standard ablative percutaneous treatments?, *Hepatobiliary Surgery and Nutrition*, **2**(4): 184–187, doi: 10.3978/j.issn.2304-3881.2013.05.02.

29. Zhang L., Rao F., Setzen R. (2017), High intensity focused ultrasound for the treatment of adenomyosis: selection criteria, efficacy, safety and fertility, *Acta Obstetricia et Gynecologica Scandinavica*, **96**(6): 707–714, doi: 10.1111/aogs.13159.

30. Zhang X., Li K., Xie B., He M., He J., Zhang L. (2014), Effective ablation therapy of adenomyosis with ultrasound-guided high-intensity focused ultrasound, *International Journal of Gynecology & Obstetrics*, **124**(3): 207–211, doi: 10.1016/j.ijgo.2013.08.022.